Enhancement of Wettability and Dissolution Properties of Cilostazol Using the Supercritical Antisolvent Process: Effect of Various Additives

Min-Soo Kim, Jeong-Soo Kim, and Sung-Joo Hwang*

Center for Nanotechnology-Based New Drug Dosage Form, College of Pharmacy, Chungnam National University; 220 Gung-dong, Yuseong-gu, Daejeon 305–764, Republic of Korea.
Received June 8, 2009; accepted November 7, 2009; published online November 18, 2009

The aim of this study was to improve wettability and dissolution rate of a poorly water-soluble drug, cilostazol, using the supercritical antisolvent (SAS) process. The solid state of particles precipitated from dichloromethane containing additives, including poloxamer 188, poloxamer 407, TPGS 1000, Gelucire® 44/14 and Gelucire® 50/13, in supercritical CO_2 medium were characterized by differential scanning calorimetry (DSC), powder X-ray diffraction (PXRD), FT-IR, particle size analysis, contact angle, and dissolution. Interestingly, the morphology of SAS particles processed with TPGS 1000, Gelucire® 44/14 and Gelucire® 50/13 changed to plate- or leaflet-shaped. Furthermore, the particle sizes of cilostazol processed with Gelucire® 44/14 and Gelucire® 50/13 were increased compared to cilostazol processed without additives. Poloxamer 188 and poloxamer 407 were superior in increasing the dissolution rate due to decreased particle size, the resulting increased surface area, and improved wettability. Micronization with the supercritical antisolvent process resulted in a significant decrease in mean particle size, and wettability of cilostazol was increased by using small amounts of hydrophilic additives.

Key words cilostazol; supercritical fluid; micronization; poorly water-soluble drug; additive

Particle formation processes based on the use of supercritical fluids functioning as solvents or anti-solvents have been introduced as a viable means of controlling particle formation. Compared to traditional organic-solvent-based processes, these methods offer advantages, including reduction in residual solvents. Supercritical CO_2 (SC-CO_2) is the most widely used supercritical fluid because of its mild critical conditions (T_c=31.1 °C, P_c=7.38 MPa), non-toxicity, non-flammability, and low price.[1,2)]

In the pharmaceutical industry, supercritical fluid technology using carbon dioxide is used to modify the solid state properties of active pharmaceutical ingredients (APIs), such as characteristics of particles (size, shape, surface, crystal structure and morphology), crystallinity, and polymorphisms related to dissolution rate and bioavailability.[3—7)] Many researchers have employed supercritical fluid techniques for micronization and for recrystallization of various APIs.[2,4,8,9)] Recently, Perrut and colleagues reported that in some cases, after a supercritical fluid process, the dissolution rates of poorly water-soluble APIs remained in the same order of magnitude, due to re-agglomeration and wetting problems, despite a reduction in particle size and increase in surface area.[10)] They emphasized the use of hydrophilic pharmaceutical excipients to enhance wettability.[11)] Various hydrophilic additives, such as poloxamers, hydroxypropyl methylcellulose (HPMC), polyethylene glycol (PEG) and polyvinyl pyrrolidone (PVP), have been used to enhance dissolution properties of poorly water-soluble APIs.[11—17)] However, the use of relatively large amounts of hydrophilic additives could lead to unwanted results, including formation of thermodynamically unstable amorphous forms and an increase in total weight of the dosage form in the development of a drug formulation. Recently, Jarmer and coworkers reported a method to selectively modify crystal habit through the use of poly(sebacic anhydride) as a growth inhibitor when an API is processed using precipitation with a compressed anti-solvent (PCA) process.[18)]

In a previous study, we investigated the effect of process parameters on the micronization of the poorly water-soluble compound cilostazol using a supercritical antisolvent process (SAS).[19)] Here we used cilostazol as a model drug and processed it by SAS with very small amounts of various additives, with the aim of increasing its wettability and dissolution rate. The solid state of particles precipitated from dichloromethane containing additives in SC-CO_2 medium were characterized by differential scanning calorimetry (DSC), powder X-ray diffraction system (PXRD), FT-IR, particle size analysis, scanning electron microscopy (SEM), contact angle, and dissolution.

Experimental

Materials Cilostazol (99.9%) was obtained from Hawil Pharm Co., Ltd. (South Korea). Carbon dioxide (CO_2) with high purity of 99.99% was supplied by Myungsin General Gas Co., Ltd. (South Korea). Poloxamer 188 (HLB: 29, melting point: 52—57 °C) and poloxamer 407 (HLB: 22, melting point: 52—57 °C) (BASF, Germany), D-α-tocopheryl polyethylene glycol 1000 succinate (TPGS 1000, HLB: 13, melting point: 37—41 °C) (Eastman Chemical Co., Kingsport, U.S.A.), Gelucire® 44/14 (HLB: 14, melting point: 42—46 °C) and Gelucire® 50/13 (HLB: 13, melting point: 46—51 °C) (Gattefossé, Saint Priest Cedex, France) were used. All organic solvents were HPLC grade. All other chemicals were analytical grade and double-distilled water was used throughout the study.

Precipitation Experiments The SAS process was performed as previously described.[15,19)] The drug/additives solutions (ratio 99/1, 100 mg/ml) were prepared by dissolving cilostazol and additives with dichloromethane. The solutions were then sprayed into the particle precipitation vessel through the inner capillary of a two-flow ultrasonic spray nozzle (Sonimist® HSS-600-1, Misonix Inc., NY, U.S.A.). Meanwhile, the SC-CO_2 was pumped to the top of the particle precipitation vessel through the outer capillary of the nozzle using an ISCO syringe pump (Model 260D). During particle precipitation, operating pressure and temperature were fixed at 40 °C and 12 MPa. The flow rates of SC-CO_2 and the drug solutions were 30 ml/min and 0.5 ml/min, respectively. After the spraying of the drug solutions and washing processes were completed, the precipitation vessel was slowly depressurized down to atmospheric pressure and the particles were collected on the wall and bottom of the vessel.

Analysis and Characterization The drug content in the processed samples was determined by HPLC. A sample of approximately 100 mg was dissolved in 100 ml ethanol. This sample solution was further diluted ten times

* To whom correspondence should be addressed. e-mail: sjhwang@cnu.ac.kr

with ethanol. Chromatographic analyses were performed on a Waters HPLC system consisting of a pump (Model 600), an auto-sampler (Model 717 plus), and UV detector (Model 486 Tunable Absorbance Detector). The C_{18} reverse phase column (Xterra, 5 μm, 4.6 mm×250 mm, Waters) was used at room temperature. The mobile phase consisted of water : acetonitrile (40 : 60) and was pumped at a flow rate of 1.0 ml/min. The injection volume was 20 μl. The signal was monitored at 254 nm. Analysis of the residual solvent was carried out on a Shimadzu 2010 model gas chromatograph (Shimadzu, Japan) equipped with a flame ionization detection (FID) system. The morphology of particles was examined by scanning electron microscopy (SEM; JSM-7000F, Jeol Ltd., Japan). X-Ray diffraction patterns were recorded on a Rigaku Powder X-ray diffraction system (Model D/MAX-2200 Ultima/PC, Japan). The X-ray source was a Cu$K\alpha$ radiation (λ=0.15418 nm), which was operated at 40 kV and 45 mA. Differential scanning calorimetry measurements were carried out using a DSC S-650 (Scinco Co. Ltd., Korea). FT-IR spectra were obtained on an FT-IR spectrometer (Bruker FT-IR: Tensor 27, Germany) using the attenuated total reflectance method. The particle sizes and distributions of samples were determined with a Sympatec laser diffraction analyzer (HELOS/RODOS, Clausthal-Zellerfeld, Germany) consisted of a laser sensor HELOS and a RODOS dry-powder air-dispersion system. The specific surface area was determined using the gas adsorption method (ASAP 2010, Micromeritics Instrument Corporation, U.S.A.). The contact angle was measured by the sessile drop technique using a drop shape analysis system (DSA100, Krüss GmbH, Germany). A compressed disc of the powder (200 mg) was made at 30 kN. The contact angle between the disc and a single drop of water (25 μl) was determined after the droplet was put onto the disc. Dissolution tests were performed using a USP XXIII rotating paddle apparatus with VK 7000 dissolution testing station and VK 750d heater/circulator (Vankel, U.S.A.) at 37 °C and a rotating speed of 50 rpm in 900 ml of pH 1.2 simulated gastric fluids (without pepsin) with 0.3% w/v sodium lauyl sulfate. Accurately weighed samples containing the equivalent of 50 mg cilostazol were dispersed in the dissolution medium. Then, 2 ml of aliquot samples were collected at different time intervals and analyzed by HPLC.

Results and Discussion

Morphology The SEM images showed agglomerates of sub-micron- to micron-sized particles with particle sizes of the SAS processed particles decreased significantly compared to the starting material (Fig. 1). It is clear from SEM images that the addition of additives had considerable effect on the shapes of cilostazol particles. The common crystal form of cilostazol is needle-shaped with a rough surface, whereas the SAS processed particles with TPGS 1000, Gelucire® 44/14 and Gelucire® 50/13 changed to plate- or leaflet-shaped. However, the morphologies of SAS processed particles with or without poloxamer 188 and poloxamer 407 were similar.

Solid-State Characterization Figure 2 represents the X-ray diffraction patterns of the cilostazol before and after processing with SAS. Neither appearance of new peaks or disappearance of peaks was detected in the SAS processed cilostazol. In Fig. 2, the locations (2θ) of every peak are identical, while the relative integrated intensity of the peaks varies. The intensities of peaks in particles with Gelucire® 44/14, Gelucire® 50/13 and TPGS 1000 were higher than that of the others. This could be due to higher crystal perfection, or to different preferred orientations of the crystals in the sample holder because of their different crystal habits. Preferred orientation is a condition in which the distribution of crystal orientation is non-random and a specific crystalline frame may tend to cluster to a greater or lesser degree about some particular orientation.[20] In SEM images (Fig. 1), these samples were plate- or leaflet-shaped. The abundance of the planes exposed to the X-ray source would have been altered, producing the change in the relative intensities of the

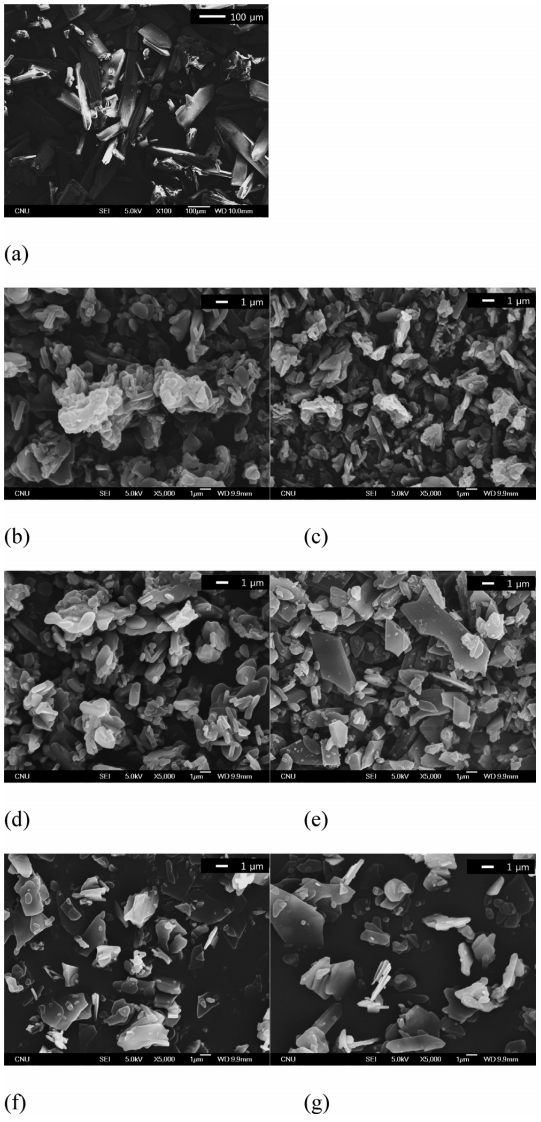

Fig. 1. SEM Images of Unprocessed Cilostazol (a), SAS Processed Cilostazol (b) and SAS Processed Cilostazol with Poloxamer 188 (c), Poloxamer 407 (d), TPGS 1000 (e), Gelucire® 44/14 (f) and Gelucire® 50/13 (g)

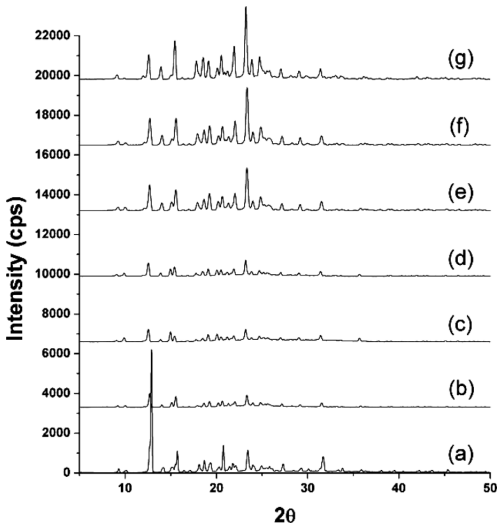

Fig. 2. Powder X-Ray Diffractograms of Unprocessed Cilostazol (a), SAS Processed Cilostazol (b), and SAS Processed Cilostazol with Poloxamer 188 (c), Poloxamer 407 (d), TPGS 1000 (e), Gelucire® 44/14 (f) and Gelucire® 50/13 (g)

peaks.[21,22] The samples recrystallized from dichloromethane containing additives in SC-CO_2 medium as well as the unprocessed sample exhibited identical IR spectra, which indicated that the altered X-ray diffraction patterns for these samples were not associated with changes at the molecular level (data not shown).

Figure 3 shows the DSC thermograms of cilostazol before and after processing with SAS, as summarized in Table 1. Recently, Stowell and colleagues[23] reported three different polymorphs of cilostazol (Form A, B and C) with melting points of 159 °C, 136 °C and 146 °C, respectively. In our study, the cilostazol did not change its crystal form during the SAS process. In addition, an ANOVA test showed no significant difference in onset and fusion temperature obtained for various cilostazol particles. However, there was a significant difference in the enthalpy of fusion ($p<0.05$). The decrease in enthalpy of fusion indicated a decrease in crystallinity. The crystallinity of cilostazol was slightly decreased during SAS process. Generally, the crystallinity of a pharmaceutical substance has an effect on its dissolution and bioavailability.[24]

The issue of solvent residues is also of interest for pharmaceutical products. GC analysis revealed a dichloromethane residual in the processed particles of less than 50 ppm. This is a very good result considering that the permitted dichloromethane concentration limit in drugs is 600 ppm, as reported by the ICH guidelines.[25] HPLC analysis confirmed that no chemical degradation occurred in the drug after the SAS process. It can be concluded that precipitation of cilostazol from supercritical carbon dioxide did not cause any polymorphic changes, and reduced crystallinity and crystal habit modification were observed.

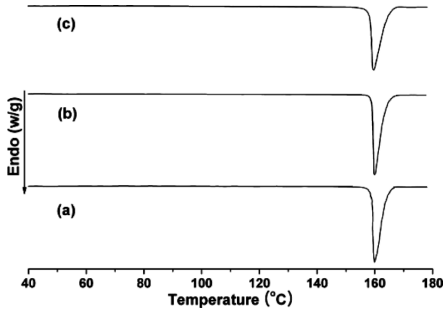

Fig. 3. DSC Thermograms of Unprocessed Cilostazol (a), SAS Processed Cilostazol (b) and SAS Processed Cilostazol with Poloxamer 188 (c)

Dissolution Study Figure 4 shows the dissolution profiles of cilostazol in dissolution medium under sink conditions ($C<0.2C_s$). Table 2 summarizes the dissolution profiles of raw cilostazol and processed cilostazol, in terms of dissolution efficiency (D.E.) at 60 min and Hixon–Crowell cube-root equation release constant (K_β). All processed cilostazol exhibited faster dissolution rates than the raw drug, with approximately 5.4 and 7.2 times increase in dissolution efficiency ($D.E._{\cdot 60}$). The ANOVA test found significant differences among the samples ($p<0.001$), and the release constants (K_β) increased in following order: raw drug< Gelucire® 50/13=Gelucire® 44/14<without additive=TPGS 1000<poloxamer 407=poloxamer 188 (ranked by the Student–Newman–Keuls test). The cilostazol samples processed

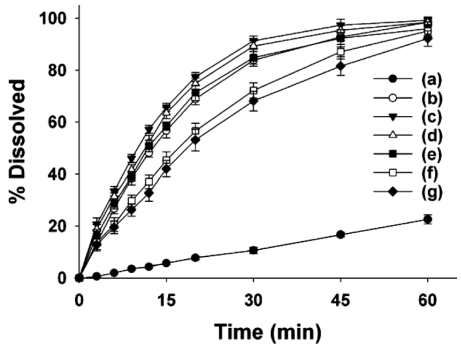

Fig. 4. Dissolution Profiles of Unprocessed Cilostazol (a), SAS Processed Cilostazol (b) and SAS Processed Cilostazol with Poloxamer 188 (c), Poloxamer 407 (d), TPGS 1000 (e), Gelucire® 44/14 (f) and Gelucire® 50/13 (g)

Table 2. The Dissolution Efficiency at 60 min and Hixon–Crowell Cube-Root Equation Release Constant of Raw Material and SAS Processed Particles with or without Various Additives

Samples	$D.E._{\cdot 60}$ [a,b]	Release constant [a,c]
Raw material	10.65±3.68	$1.33\times10^{-3}\pm5.77\times10^{-5}$ (0.9959)[d]
No additives	70.48±0.69	$1.57\times10^{-2}\pm7.57\times10^{-4}$ (0.9956)
Poloxamer 188	76.39±0.95	$1.94\times10^{-2}\pm9.07\times10^{-4}$ (0.9920)
Poloxamer 407	74.34±0.88	$1.81\times10^{-2}\pm1.00\times10^{-3}$ (0.9946)
TPGS 1000	71.09±0.77	$1.64\times10^{-2}\pm1.17\times10^{-3}$ (0.9902)
Gelucire® 44/14	62.54±0.60	$1.19\times10^{-2}\pm9.07\times10^{-4}$ (0.9952)
Gelucire® 50/13	58.33±0.56	$1.08\times10^{-2}\pm1.02\times10^{-3}$ (0.9940)

a) Mean±S.D., $n=6$. *b*) Calculated from the area under the dissolution curve at 60 min and expressed as % of the area of the rectangle described by 100% dissolution in the same time. *c*) Hixon–Crowell cube-root equation in which $1-(1-M_t/M_0)^{1/3}$ is plotted against time (M_t, drug content remaining after time t; M_0, original content of drug). *d*) Determination coefficient (r^2).

Table 1. DSC Thermograms Data and X-Ray Diffraction Data of Raw Material and SAS Processed Particles with or without Various Additives

Samples	DSC					X-ray diffraction data (2θ)
	Drug content[a] (%)	Onset temperature[b] (°C)	Fusion temperature[b] (°C)	Enthalpy of fusion[b] (ΔH, J/g)	Relative crystallinity[b,c] (%)	
Raw material	—	158.89±0.17	160.14±0.16	129.63±4.22	—	12.8, 15.7, 20.7, 23.4, 31.7
No additive	—	158.90±0.28	159.98±0.32	112.25±3.07	86.60±2.36	12.7, 15.5, 20.6, 23.3, 31.6
Poloxamer 188	98.91±0.31	158.86±0.18	159.91±0.22	109.78±4.01	85.62±3.12	12.5, 15.4, 20.5, 23.2, 31.4
Poloxamer 407	99.25±0.20	158.89±0.21	159.95±0.26	110.51±4.19	85.89±3.26	12.5, 15.4, 20.5, 23.2, 31.4
TPGS 1000	99.07±0.43	158.93±0.22	160.07±0.17	112.08±2.34	87.28±1.84	12.7, 15.5, 20.6, 23.3, 31.5
Gelucire® 44/14	99.10±0.51	158.95±0.26	160.01±0.21	118.92±2.87	92.58±2.23	12.7, 15.6, 20.6, 23.3, 31.5
Gelucire® 50/13	99.09±0.50	158.99±0.19	160.04±0.21	118.50±4.07	92.26±3.17	12.6, 15.4, 20.5, 23.3, 31.4

a) Mean±S.D., $n=5$. *b*) Mean±S.D., $n=4$. *c*) $\Delta H_{sample}/\Delta H_{raw}\times100f$, f: correct factor related drug content.

Table 3. Particle Size, Specific Surface Area and Contact Angle of Raw Material and SAS Processed Particles with or without Various Additives

Samples	Volume mean particle size[a] (μm)	Specific surface area[a] (m^2/g)	Contact angle[b] (°)	
			10 s	180 s
Raw material	47.95±5.58 (3.15)[c]	0.49±0.02	65.5±2.9	60.7±2.7
No additive	3.12±0.10 (1.79)	4.09±0.06	62.1±2.3	57.8±2.4
Poloxamer 188	2.17±0.28 (1.75)	4.30±0.08	56.1±3.8	47.9±3.6
Poloxamer 407	3.03±0.27 (1.94)	4.11±0.09	54.5±3.6	49.5±3.3
TPGS 1000	4.76±0.19 (2.14)	3.27±0.03	54.9±4.6	46.5±3.5
Gelucire® 44/14	5.77±0.07 (2.30)	2.32±0.04	57.1±1.9	51.8±3.3
Gelucire® 50/13	6.41±0.07 (2.38)	2.10±0.02	58.3±2.2	52.5±2.6

a) Mean±S.D., $n=3$. *b*) Mean±S.D., $n=6$. *c*) SPAN$=(d_{90}-d_{10})/d_{50}$, where d_{10}, d_{50} and d_{90} are the diameter sizes and the given percentage value is the percentage of particles smaller than that size.

with poloxamer 188 and 407 had the highest dissolution rates, caused by the decreased crystallinity, the decreased particle size and thus increased surface area, and the improved wettability, reflected by the contact angles, as described in Table 3. However, the dissolution rate of cilostazol with Gelucire® 44/14 and 50/13 were significantly decreased, due to the increased particle size and distribution, despite the higher wettability compared to cilostazol without additives.

The lower contact angles or higher hydrophilicities suggest a change in surface properties of the precipitated cilostazol. It was expected that the addition of additives would affect particle formation processes, such as supersaturation, nucleation and crystal growth in SC-CO_2 medium, resulting in changes in surface properties and shape of particles without polymorphic changes.

In conclusion, micronization with supercritical antisolvent process resulted in a significant decrease in mean particle size. Wettability of cilostazol was increased by using a small amount of hydrophilic additives. Interestingly, particle sizes of cilostazol processed with Gelucire® 44/14 and 50/13 were increased compared to cilostazol processed without additives. Among the additives studied here, poloxamer 188 and poloxamer 407 proved to be superior in increasing the dissolution rate due to the decreased particle size and thus increased surface area, and the improved wettability.

Acknowledgments This work was supported by the Korea Science and Engineering Foundation (KOSEF) grant funded by the Korea government (MOST) (No. R172008025010010 2008).

References

1) Vemavarapu C., Mollan M. J., Lodava M., Needham T. E., *Int. J. Pharm.*, **292**, 1—16 (2005).
2) Subramaniam B., Rajewski R. A., Snavely K., *J. Pharm. Sci.*, **86**, 885—890 (1997).
3) Dehghani F., Foster N.R., *Curr. Opin. Solid State Mater. Sci.*, **7**, 363—369 (2003).
4) Pasquali I., Bettini R., Giordano F., *Eur. J. Pharm. Sci.*, **27**, 299—310 (2006).
5) Park H. J., Kim M.-S., Lee S., Kim J.-S., Woo J.-S., Park J.-S., Hwang S.-J., *Int. J. Pharm.*, **328**, 152—160 (2007).
6) Jun S. W., Kim M.-S., Kim J.-S., Park H. J., Lee S., Woo J.-S., Hwang S.-J., *Eur. J. Pharm. Biopharm.*, **66**, 413—421 (2007).
7) Lee S., Nam K., Kim M.-S., Jun S. W., Park J.-S., Woo J. S., Hwang S.-J., *Arch. Pharm. Res.*, **28**, 866—874 (2005).
8) Reverchon E., *J. Supercrit. Fluids*, **15**, 1—21 (1999).
9) Jung J., Perrut M., *J. Supercrit. Fluids*, **20**, 179—219 (2001).
10) Perrut M., Jung J., Leboeuf F., *Int. J. Pharm.*, **288**, 3—10 (2005).
11) Perrut M., Jung J., Leboeuf F., *Int. J. Pharm.*, **288**, 11—16 (2005).
12) Senčar-Božič P., Srčič S., Knez Ž., Kerč J., *Int. J. Pharm.*, **148**, 123—130 (1997).
13) Van Nijlen T., Brennan K., Van den Mooter G., Blaton N., Kinget R., Augustijns P., *Int. J. Pharm.*, **254**, 173—181 (2003).
14) Meure L. A., Warwick B., Dehgani F., Regtop H. L., Foster N. R., *Ind. Eng. Chem. Res.*, **43**, 1103—1112 (2004).
15) Jun S. W., Kim M.-S., Jo G. H., Lee S., Park J.-S., Woo J. S., Hwang S.-J., *J. Pharm. Pharmacol.*, **57**, 1529—1537 (2005).
16) Won D.-H., Kim M.-S., Lee S., Park J.-S., Hwang S.-J., *Int. J. Pharm.*, **301**, 199—208 (2005).
17) Majerik V., Charbit G., Badens E., Horváth G., Szokonya L., Bosc N., Teillaud E., *J. Supercrit. Fluids*, **40**, 101—110 (2007).
18) Jarmer D. J., Lengsfeld C. S., Anseth K. S., Randolph T. W., *J. Pharm. Sci.*, **94**, 2688—2702 (2005).
19) Kim M.-S., Lee S., Park J.-S., Woo J.-S., Hwang S.-J., *Powder Technol.*, **177**, 64—70 (2008).
20) Cullity B. D., "Elements of X-ray Diffraction," 2nd ed., Addison-Wesley Publishing, Massachusetts, 1978.
21) Marshall P. V., York P., *Int. J. Pharm.*, **55**, 257—263 (1989).
22) Nokhodchi A., Bolourtchian N., Dinarvand R., *Int. J. Pharm.*, **250**, 85—97 (2003).
23) Stowell G. W., Behme R. J., Denton S. M., Pfeiffer I., Sancilio F. D., Whittall L. B., Whittle R. R., *J. Pharm. Sci.*, **91**, 2481—2488 (2002).
24) Vippagunta S. R., Brittain H. G., Grant D. J. W., *Adv. Drug Deliv. Rev.*, **48**, 3—26 (2001).
25) ICH, *Fed. Regist.*, **68**, 64352—64353 (1997).